DOI: 10.26599/FSHW.2026.9251038

Contents lists available at SciOpen

Food Science and Human Wellness

journal homepage: https://www.sciopen.com/journal/2097-0765

China Food Publishing Co.

Unveiling the molecular secrets: How *Levilactobacillus brevis* PDD-5 lowers uric acid levels

Jue Xu [a, b, c1], Yujiao Lou [a1], Tao Zhang [b], Mingzhen Liu [b], Qiwei Du [b], Zhen Wu[b], Xiefei Li [a *], Daodong Pan [b *]

[a] *The Key Laboratory of Environmental Pollution Monitoring and Disease Control, Ministry of Education, Guizhou Provincial Engineering Research Center of Ecological Food Innovation, School of Public Health, Guizhou Medical University, Guiyang 550025, China*

[b] *State Key Laboratory for Quality and Safety of Agro-Products, College of Food Science and Engineering, Ningbo University, Ningbo, Zhejiang 315211, China*

[c] *Key Laboratory of Natural Anti-aging Product Mining and Biosynthesis of Shaanxi Higher Education Institutes, Applied Research Institute of Life Sciences, Xi'an International University, Xi'an, 710077, China*

ABSTRACT: A high-purine diet readily induces hyperuricemia, whereas certain lactic acid bacteria (LAB) can absorb and metabolize purines, thereby modulating uric acid levels. However, studies elucidating the molecular mechanisms by which lactic acid bacteria lower uric acid levels remain limited. In this study, we investigated *Levilactobacillus brevis* PDD-5, a strain previously shown to alleviate hyperuricemia through efficient purine absorption. Comprehensive metabolic and transcriptomic analyses were performed to compare *L. brevis* PDD-5 with a non-uric-acid-lowering strain. Using HPLC–MS/MS–based targeted metabolomics, we identified significant differences in purine nucleoside degradation between the two strains. Transcriptomic profiling revealed that *L. brevis* PDD-5 activates purine catabolism *via* upregulation of the *deoD* gene, which encodes purine nucleoside phosphorylase, thereby facilitating nucleoside-to-base conversion. Xanthine served as a key substrate promoting the *de novo* purine synthesis pathway and remained active under purine-rich conditions, likely because of transcriptional derepression of the *purR* regulator. These findings elucidate the molecular framework of the uric acid–lowering mechanism of *L. brevis* PDD-5 and provide a theoretical foundation for the development of safe, effective LAB-based interventions against hyperuricemia.

Keywords: Lactic acid bacteria; purine metabolism; hyperuricaemia; metabolomics; transcriptomics

1. Introduction

Hyperuricemia is the second commonest metabolic disorder after type II diabetes, and the average age of patients with hyperuricaemia has decreased substantially [1]. As more young people tend to be sub-healthy due to stress, staying up late, drinking, and smoking, assessing the importance of eating healthy meals is becoming more and more important in this fast-paced era. Purine nucleosides can be found in many foods and beverages, such as meat, fish, and beer [2]. Excessive purine intake will break down into uric acid in the body and accumulate in the blood, causing various complications such as hyperuricemia and gout [3, 4].

[1]authors contributed equally to this work
[*]**Corresponding author**
daodongpan@163.com. xiefeili.edu@gmail.com

Received 24 April 2025
Received in revised from 10 June 2025
Accepted 18 November 2025

While conventional therapeutics like allopurinol provide symptomatic relief, their severe side effects necessitate safer alternatives. Emerging evidence positions lactic acid bacteria (LAB) as promising microecological regulators for uric acid homeostasis, though their precise molecular mechanisms remain enigmatic.

LAB demonstrates multifaceted therapeutic potential through immunomodulation, gut barrier enhancement, and xenobiotic detoxification [5]. Notably, specific strains exhibit unique purine-metabolizing capabilities, such as *Lactobacillus sakei* degraded fundamental nucleosides (inosine/adenine), while gut-derived microbes employ ribonuclease-mediated purine catabolism [6]. Our prior work identified *L. brevis* PDD-5 (CGMCC 20573) as a particularly effective hyperuricemia mitigator, contrasting with the limited purine absorption capacity of the psychobiotic strain *L. brevis* 54 [7]. These findings align with Zhao *et al.*'s report on *Lacticaseibacillus rhamnosus* Fmb14 from traditional fermented dairy [8], collectively suggesting strain-specific purine metabolism as a key therapeutic determinant. An increasing number of LAB species have been identified as capable of alleviating hyperuricemia through the uptake of degraded purine nucleosides [9, 10]. Nevertheless, the molecular architecture governing LAB-mediated purine processing—particularly nucleoside uptake efficiency and catabolic pathway regulation—remains poorly characterized.

Recent advances in multi-omics integration provide unprecedented resolution for deciphering microbial metabolic networks [11]. Wang *et al.* [12] exemplified this approach by combining metabolomics and gut microbiota profiling to elucidate nuciferine's anti-hyperuricemic mechanisms. Our group previously employed transcriptomics to delineate nitrite degradation pathways in *Limosilactobacillus fermentum* RC4 [13]. Building on these methodological frameworks, we herein implement an integrated full-targeted metabolomics and transcriptomics strategy to unravel the purine regulatory machinery of *L. brevis* PDD-5. Through synchronized LC-MS/MS-based metabolite profiling and global transcript analysis, we systematically identify rate-limiting enzymes in nucleoside catabolism, transmembrane transporters governing purine uptake efficiency, and regulatory networks coordinating uric acid reduction. This dual-omics dissection not only advances LAB mechanistic understanding but also establishes a paradigm for developing precision probiotics against metabolic disorders.

2. Materials and Methods

2.1 Materials

L. brevis PDD-5 and *L. brevis* 54 were screened by our laboratory and stored in the China General Microbiological Culture Collection Center (CGMCC) with registration numbers CGMCC 20573 and CGMCC 15954, respectively. Inosine, guanosine, and allopurinol were obtained from Beijing Solarbio Science & Technology Co.,Ltd. Tripotassium phosphate (K_3PO_4) was obtained from Lingfeng Chemical Reagent Co., LTD (Shanghai, China). RNA Bacteria Kit was purchased from Sigma (Merck, Darmstadt, Germany). Purine nucleoside buffer is a standard assay mixture composed of 12.6 mM inosine, 12.6 mM

guanosine, and 0.1 M sodium phosphate buffer (pH 7.0). All primers were obtained from Sangon Biotech (Shanghai) Co., Ltd.

2.2 Metabolite extraction of bacterial strains in high-purine environments

After being activated for two generations, *L. brevis* 54 and *L. brevis* PDD-5 were inoculated in MRS liquid medium with a 1% (v/v) inoculum and incubated at 37°C for 24 h, respectively. The cultures were then centrifuged at 8,000 rpm for 10 minutes to separate the bacterial cells from the supernatant. The supernatant was collected and resuspended in an equal volume of sterile phosphate buffer and purine nucleoside buffer for 1 h. After this incubation, the mixtures were centrifuged again at 8,000 rpm for 10 min to obtain the final supernatant, which was then analyzed for metabolome.

The cultures of *L. brevis* 54 and *L. brevis* PDD-5 in MRS medium were designated as L54M and P_M, respectively. The cultures of *L. brevis* 54 and *L. brevis* PDD-5 in purine nucleoside buffer were designated as L54H and P_H, respectively. Each group included six biological replicates, and the supernatant samples from each group were centrifuged for subsequent untargeted metabolomics analysis. Six replicates were used to enhance statistical reliability and capture metabolic variability across conditions [14]. Subsequently, representative conditions identified from metabolomic profiling were used for transcriptomic analysis with three biological replicates, consistent with standard RNA-seq experimental design.

2.3 Metabolite analysis based on HPLC-MS/MS

2.3.1 Sample extraction and LC–MS/MS analysis

To extract metabolites, 100 μL of supernatant was mixed with 400 μL of a methanol: acetonitrile (1: 1, v/v) solution. The mixture was subjected to ultrasonication at 40 kHz for 30 min at 5°C. Subsequently, the samples were incubated at -20°C for 30 min to precipitate proteins. Following centrifugation at 13,000 × g at 4°C for 15 min, the supernatant was carefully transferred to new microtubes and dried under a gentle stream of nitrogen gas. For HPLC-MS/MS analysis, the dried samples were reconstituted in 100 μL of an acetonitrile: water (1: 1, v/v) loading solution *via* brief sonication in a water bath maintained at 5°C. The reconstituted samples were then centrifuged at 13,000 × g at 4°C for 15 min using a bench-top centrifuge. The resulting supernatant was transferred to sample vials for subsequent HPLC-MS/MS analysis [15].

Chromatographic separation was accomplished by a UHPLC-Q Exactive HF-X system (Thermo Fisher Scientific, Austin, Texas (TX), USA). Samples were separated on an ACQUITY UPLC®HSS T3 column (100 mm × 2.1 mm i.d., 1.8 μm, Waters, Massachusetts (MA), USA) with a loading volume of 2 μL at 40°C. The mobile phase A was 0.1% formic acid aqueous solution: acetonitrile (95: 5, v/v), and mobile phase B was 0.1% formic acid acetonitrile: isopropanol: water (47.5: 47.5: 5, v/v). The gradient elution was as follows: 0% B (0-0.1 min), 0-5% B (0.1-2 min), 5-25% B (2-9 min), 25-100% B (9-13 min), 100% B (13-13.1 min), 100-0% B (13.1-16 min), at a constant flow rate of 0.3 mL/min. Mass spectrometry data were collected in both positive and negative ion modes (-2,800 V and +3,500V, respectively), with normalized collision energy of 20-40-60 V. Full MS resolution was set to 70,000, and MS/MS resolution was 17,500.

Data acquisition was performed in data-dependent acquisition (DDA) mode over a mass range of 70-1,050 m/z.

2.3.2 Quality control analysis of metabolites

To ensure data reliability, a series of preprocessing steps was performed, including filtering of low-quality peaks, missing-value imputation, normalization, and quality control (QC) assessment [16]. Relative standard deviation (RSD) values of QC samples were used to evaluate instrument stability. Data were log-transformed and Pareto-scaled before statistical analysis to minimize the influence of irrelevant variation and enhance comparability among samples.

2.3.3 Comparative and multidimensional analysis

To evaluate inter- and intra-group variation, correlation heatmaps and principal component analysis (PCA) were performed to assess sample similarity and overall metabolic variation. Orthogonal partial least squares discriminant analysis (OPLS-DA) was subsequently applied to highlight group separation and identify metabolites contributing most to discrimination [17]. Differential metabolites between groups were visualized using heatmaps, PCA, and Venn diagrams.

2.3.4 Metabolite annotation

Based on the identification of all metabolites obtained by mass spectrometry, compounds were annotated by matching accurate mass, retention time, and MS/MS fragmentation spectra with the KEGG and HMDB databases [18]. Annotated metabolites were classified into biological categories according to KEGG hierarchical levels, including amino acid metabolism, carbohydrate metabolism, lipid metabolism, nucleotide metabolism, and other secondary metabolites. Metabolite classification profiles and statistical mapping were generated based on the KEGG Compound database.

2.3.5 Metabolomic data processing and KEGG pathway analysis

Raw mass spectrometry data were processed for peak alignment, normalization, and compound identification. Multivariate and univariate statistical analyses were combined to identify significantly differential metabolites. Metabolites with variable importance in projection (VIP) ≥ 1.0 from the OPLS-DA model and false discovery rate (FDR) ≤ 0.05 (Benjamini–Hochberg adjusted p-value) were defined as significantly different between groups. Metabolites with $0.05 < \text{FDR} \leq 0.10$ were considered to show potential differences and are listed as candidate metabolites. Functional classification illustrated the distribution of significantly differential metabolites across KEGG superclasses, while pathway enrichment analysis identified statistically overrepresented pathways using Fisher's exact test, followed by Benjamini–Hochberg FDR correction. Pathways with FDR ≤ 0.05 were considered significantly enriched, and because the main objective of this study was to elucidate the metabolic modulation of *L. brevis* PDD-5 under high-level conditions, KEGG analysis focused on the L54H vs P_H comparison.

2.4 Analysis of the mechanism of uric acid-lowering lactic acid bacteria based on transcriptional level

2.4.1 Extraction of RNA from strains in a high-purine environment

To study the molecular mechanism of the uric acid-lowering strain *L. brevis* PDD-5, 3 mL of *L. brevis* PDD-5 was taken, washed with PBS, and then centrifuged to collect the cells. *L. brevis* PDD-5 was inoculated with 1% (v/v) inoculum in high-purine buffer and normal MRS medium, respectively, and incubated for 1 h. Bacteria were centrifuged. The total RNA was extracted using the Hipure bacterial RNA Kit (MGI Tech Co., Ltd.).

2.4.2 Transcription and library creation

The extracted total RNA was purified to obtain mRNA, and the obtained mRNA was randomly broken and fragmented. cDNA first strand was synthesized using the fragmented mRNA as a template and random oligonucleotides as primers, and then the RNA strand was degraded by RNaseH, and the cDNA second strand was synthesized by dNTP instead of dTTP under the DNA polymerase I system using dUTP as the raw strand. The purified double-stranded cDNA was end-repaired, A-tailed, and connected to the sequencing junction, and then USERase (NEB, USA) was added to degrade the second strand of U-containing cDNA. The cDNAs of about 370-420 bp were then screened, PCR amplified, and the PCR products were purified again to finally obtain the library. After library construction, the samples were initially quantified, and the library was diluted to 1.5 ng/μl. Subsequently, the library was tested using Agilent 2100 bioanalyzer, and after meeting the expectations, accurate quantification (effective library concentration higher than 2 nM) was performed to ensure the quality of the library. After the libraries passed the test, they were sequenced on the machine, and this part was done by the Beijing Genomics Institution (BGI, China).

2.4.3 Illumina transcriptomic sequencing

RNA sequencing was performed using the Illumina HiSeq 2000 platform. Clean reads were aligned to the reference genome of *L. brevis* ATCC 14869. The number of reads was normalized to reads per kilobase per million mapped reads (RPKM) [19]. Expression levels were normalized as RPKM (reads per kilobase per million mapped reads), equivalent to FPKM (fragments per kilobase per million) for paired-end sequencing data. Differentially expressed genes (DEGs) were identified using the DEGseq package with the MA-plot-based method and the random sampling model. Significance thresholds included a false discovery rate (FDR) ≤ 0.05, a log2 fold change > 1 or < -1, and a *P-value* < 0.05. Clean RNA-seq reads were aligned to the *L. brevis* ATCC 14869 reference genome because, at the time of analysis, a high-quality and fully annotated genome of *L. brevis* PDD-5 was not available. The mapping rates of all samples (62.9–71.8%) indicated substantial sequence homology, allowing accurate gene-level and pathway-level analysis. For the transcriptomic analysis, three biological replicates were used for each condition, which is consistent with common RNA-seq experimental standards and provides sufficient statistical power for differential gene expression analysis [20]. To integrate the metabolomic and transcriptomic datasets, all data were normalized by z-score transformation before joint pathway analysis, thereby minimizing the potential influence of replicate number differences between omics layers.

For the targeted analysis of key regulatory genes (e.g., *purR*), normalized expression values (FPKM) were extracted from the RNA-seq dataset. Differential expression analysis of all genes was conducted using

the DEGseq package (v1.36.0). For selected genes of interest, group-wise comparisons were additionally performed using Welch's two-sample t-test (two-sided) when variances between groups were unequal. Reported gene-level means and standard deviations represent biological replicates (n = 3 per group). All visualizations of gene expression patterns were automatically generated within the BGI transcriptomic analysis system.

2.4.4 Quantitative reverse-transcriptase polymerase chain reaction (qRT-PCR) validation

qRT-PCR analysis was performed using a qRT-PCR (TER010-2) kit (Dingguo, Beijing, China) on the StepOne Real-Time PCR system (Applied Biosystems). Total RNA, after DNase treatment to remove genomic DNA, was reverse-transcribed into cDNA using a mixture containing 2 μL of 10× Fast RT Buffer, 2 μL of FQRT Primer Mix, 1 μL of RT Enzyme Mix, and 15 μL of RNase-free ddH_2O (procedure: 42°C for 15 min followed by 95°C for 3 min). For the qRT-PCR reaction, 50 ng of cDNA was combined with 0.3 μM of each primer, 10 μL of Super Real Premix Plus with SYBR Green I, and 1.6 μL of ROX Reference Dye, diluted to a final volume of 20 μL with RNase-free ddH_2O. The amplification protocol consisted of initial denaturation for 10 minutes, followed by 40 cycles of denaturation at 95°C for 15 s, annealing at 56°C for 15 s, and extension at 72°C for 30 s. Relative gene expression was quantified using the $2^{-\Delta\Delta CT}$ method, with the *gyrA* gene serving as the internal reference. Primers were designed using Primer 6.0 software and synthesized by Sangon Biotech (Shanghai, China). Each sample was analyzed in triplicate.

2.5 Functional annotation

The metabolite results were searched and identified against the databases HMDB (http://www.hmdb.ca/), Metlin (https://metlin.scripps.edu/), and the Majorbio database. Pathway maps were manually constructed using the Kyoto Encyclopedia of Genes and Genomes (KEGG) to represent the understanding of reaction networks and molecular interactions. Gene Ontology (GO) provides a set of dynamically updated controlled vocabularies to describe the attributes of genes and proteins within an organism, encompassing molecular functions, cellular components, and biological processes. Identified genes and proteins were classified using the KEGG database (http://www.genome.jp/kegg/) and the GO database (http://www.geneontology.org/).

2.6 Statistical analysis

Statistical analyses were conducted according to the standard procedures of each analytical platform. For metabolomic analysis, differential metabolites were determined using VIP ≥ 1.0 (OPLS-DA) and FDR ≤ 0.05. For transcriptomic analysis, DEGs were identified using DEGseq (v1.36.0), with significance thresholds of $|\log_2(\text{fold change})| > 1$, $P < 0.05$, and FDR ≤ 0.05. Data are expressed as the mean ± standard error of the mean. Group-wise comparisons of specific genes were evaluated using Welch's two-sample t-test (two-sided) when variances were unequal. Graphs were prepared using GraphPad Prism 8.0.1, and $P < 0.05$ was considered statistically significant unless otherwise stated. The replicate design (n = 6 for

metabolomics, n = 3 for transcriptomics) and normalization strategy have been widely adopted in multi-omics studies [21, 22].

3. Results

3.1 Full-target metabolism analysis of different L. brevis strains treated with high-purine cultures

3.1.1 Comparative analysis of samples

In our previous study, the degradation rates of inosine and guanosine by *L. brevis* PDD-5 were 68.86 ± 15.46% and 95.75 ± 3.30%, while the degradation rates of inosine and guanosine by *L. brevis* 54 were 39.08 ± 4.76% and 42.64 ± 6.19% (Table S1). To investigate the specificity of purine nucleoside uptake by different strains of *L. brevis* in the same genus, we opted for more precise fully targeted metabolomic analysis. The results in Figure 1A indicated that untreated *L. brevis* PDD-5 (P_M) and *L. brevis* PDD-5 treated with purine nucleoside buffer (P_H) were significantly separated by LC-MS/MS in the anion mode in the PCA plot. The untreated *L. brevis* 54 (L54M) and *L. brevis* 54 treated with purine nucleoside buffer (L54H) were also significantly separated, indicating that purine nucleoside buffer affected the growth metabolism of *L. brevis*. In addition, no separation was observed between the P_M and L54M groups, but there was a clear separation between the P_H and L54H groups. Differential metabolites between the four different groups were identified in Figure 1B. Among them, 70 differential metabolites were identified between L54H and L54M (Table S2), 75 differential metabolites were identified between P_H and P_M (Table S3), and 74 differential metabolites were identified between P_H and L54H (Table S4). In the purine metabolic pathway, the differential metabolites were inosine, guanosine, adenine, xanthine, IDP, and adenosine monophosphate in the P_H group compared to the L54H group. In addition, the sample correlation heat map (Figure 1C) reflected the similarity and abundance of metabolic composition between samples, with a clear separation between the metabolites of the strains in normal culture conditions (P_M and L54M) and those of the purine nucleoside treated strains (P_H and L54H), with no significant differences between the P_M and L54M groups, and differences between the purine nucleoside treated groups (P_H and L54H). This is consistent with the results of the PCA plot responses, and the data are reliable for each group of samples.

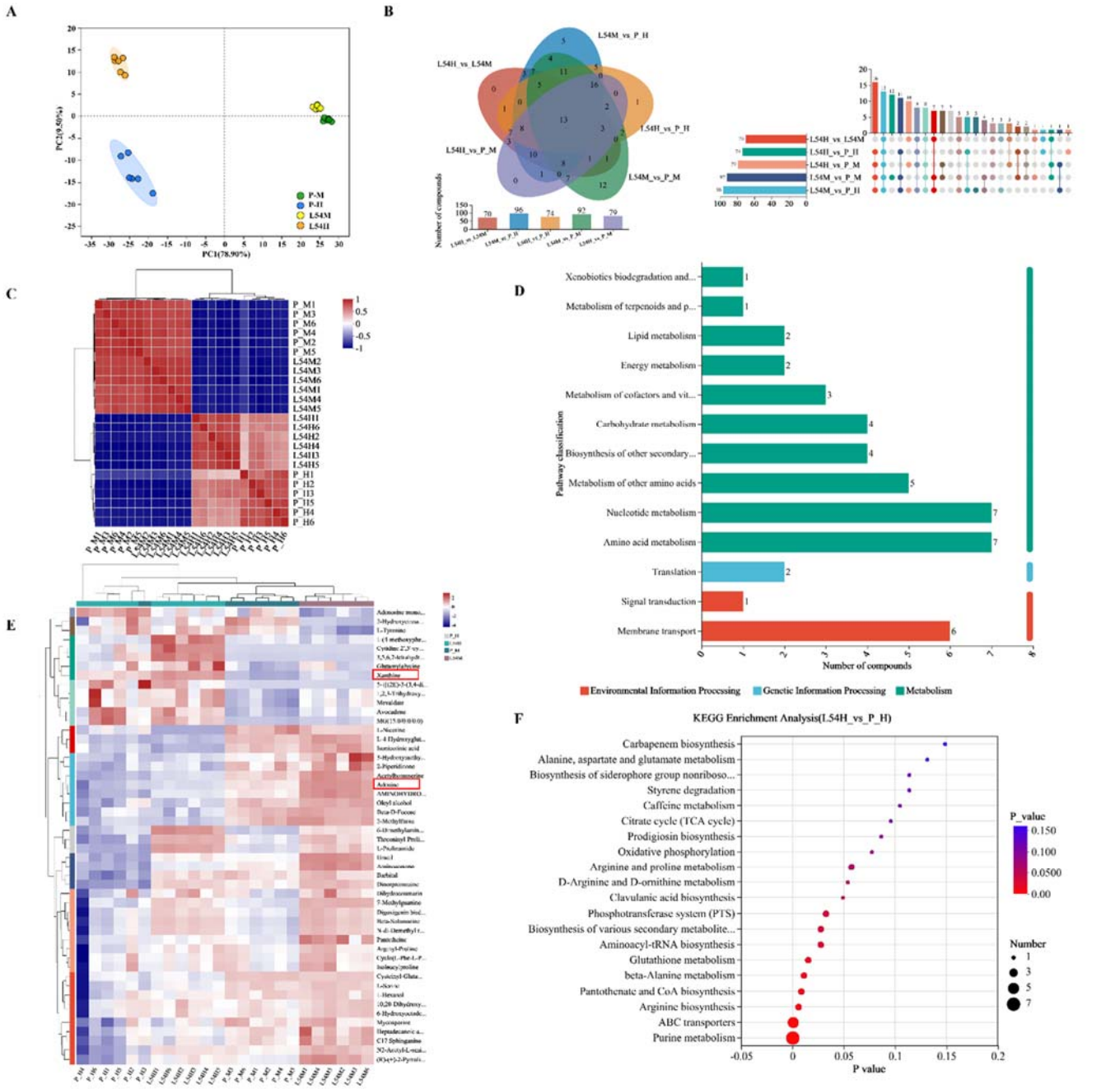

Figure 1. Comparison and analysis of samples based on untargeted metabolomics. (A) PCA score plot showing the overall distribution of metabolites in different groups. (B) Venn diagram and upset plot of metabolic sets across groups. (C) Metabolite sample correlation heatmap. A higher correlation value indicates greater similarity in metabolic composition and abundance among samples. (D) KEGG functional classification of significantly differential metabolites (VIP ≥ 1.0, FDR ≤ 0.05) between L54H and P_H. (E) Heat map of metabolites. Adenine showed higher levels in the M groups (P_M and L54M), while downstream purine metabolites such as xanthine was more abundant in the H groups (P_H and L54H). (F) KEGG pathway enrichment analysis (VIP ≥ 1.0, FDR ≤ 0.05) between L54H and P_H.

3.1.2 Metabolite annotation and KEGG pathway analysis

Metabolites identified from mass spectrometry were annotated using the KEGG database for functional classification and pathway enrichment. Most were assigned to metabolic categories, mainly involving amino acid, nucleotide, lipid, and carbohydrate metabolism (Figure 1D). Multivariate analyses (PCA and OPLS-DA) revealed clear group separation, indicating that *L. brevis* PDD-5 substantially altered the global metabolic profile (Figure 1A–C). Compared with the control groups (P_M and L54M), both high-purine

treatments (P_H and L54H) exhibited enhanced purine degradation activity, as reflected by decreased adenine and elevated xanthine levels (Figure 1E). This suggests that *L. brevis* PDD-5 actively promotes purine catabolism in response to substrate excess. To pinpoint the major metabolic shifts, univariate and multivariate analyses (VIP ≥ 1.0, FDR ≤ 0.05) identified 29 significantly different metabolites between P_H and L54H (Table 1). These metabolites were mainly enriched in purine metabolism, ABC transport, and amino acid metabolism (Figure 1F), highlighting that *L. brevis* PDD-5 preferentially regulates nucleotide turnover and purine degradation under high-purine conditions.

Table 1. Significantly differential metabolites between P_H and L54H identified based on VIP ≥ 1.0 and FDR ≤ 0.05.

Compound	P_value	FDR
Guanosine	2.416E-7	2.839E-5
D-Glucaro-1,4-lactone	5.937E-5	0.0022
Phenylacetaldehyde	2.147E-10	1.149E-7
Dinorpromazine	4.29E-9	1.216E-6
Acetylcholine	9.103E-6	0.0004617
1-(4-methoxyphenyl) pentan-3-ol	1.1E-6	8.685E-5
N-Acetyl-2,3-dihydro-1H-pyrrole	5.948E-7	5.511E-5
Sterebin B	0.002862	0.04542
Glutamyltryptophan	1.264E-7	1.74E-5
N-Acetyl-b-glucosaminylamine	5.363E-9	1.292E-6
N2-Acetyl-L-ornithine	3.358E-12	4.044E-9
5'-Deoxy-5'-(methylthio)adenosine	0.002826	0.04539
Cysteinylglycine	0.001892	0.03314
Biotin amide	3.705E-5	0.001463
Barbital	2.684E-6	0.0001701
L-Carnitine	0.001146	0.02272
1-Pyrroline	6.512E-7	5.704E-5
L-Prolinamide	2.059E-11	1.417E-8
Cysteinyl-Serine	0.001371	0.02632
Harmalol	6.288E-8	9.468E-6
6-Dimethylaminopurine	2.137E-6	0.000143
N2-Acetyl-L-aminoadipate	0.0002039	0.005647
Glucosamine	4.894E-6	0.0002777
Threoninyl-Proline	2.308E-6	0.0001523
1-Methylhypoxanthine	2.876E-5	0.001216
Cytidine 2',3'-cyclic phosphate	0.0001036	0.003372
L-Nicotine	0.0005705	0.01309
L-Proline	0.0003116	0.008037
3,5,6,7-tetrahydroxy-2-(3-methoxyphenyl)-3,4-dihydro-2H-1-benzopyran-4-one	0.0003694	0.009318

3.2 Analysis of the key genes of L. brevis PDD-5

After the low-scoring sequenced reads were removed, Illumina sequencing generated14413300, 18534550, 16899212, and 15002034, 15271622, 12131462 total clean reads for strains PDD-5 in a normal environment (Y, n = 3) and strain PDD-5 in a purine nucleoside environment (P, n = 3), with mapped percentages of 70.02, 70.06, 70.43 and 62.94, 71.75, 64.79 % to the genome of *L. brevis* ATCC 14869, respectively. Identification of differentially expressed genes in both groups revealed that a total of 1158 genes were clearly expressed in the P group (*L. brevis* PDD-5 in a purine nucleoside environment) compared with the Y group (*L. brevis* PDD-5 in a normal environment), of which 605 genes were significantly up-regulated and 553 genes were significantly down-regulated (Figure 3A). Due to the large number of

differential genes, it was not possible to quickly filter out eligible genes with statistically significant differences, so the differential gene pairs were plotted as volcano maps (Figure 3B). In Figure 3B, the points located at the top indicated a highly significant statistical difference. According to the above results, we further performed KEGG and GO enrichment analysis for each group of differentially expressed genes. As shown by the KEGG pathway classification Figure 3C, the differential genes of *L. brevis* PDD-5 were mainly concentrated in metabolic processes, and we plotted the top 20 metabolic pathways enriched for significantly differentially expressed genes in Figure 3D. Results of GO showed enrichment in cellular components, molecular functions, and biological processes (Figure 3E-F). The results of GO and KEGG enrichment analysis of the significantly different genes of *L. brevis* PDD-5 and *L. brevis* ATCC 14869 above were used to screen six significantly enriched pathways with a threshold of $P \leq 0.05$, as shown in Table 2, including purine metabolism, ABC transport, galactose metabolism, population sensing, fatty acid metabolism, and microbial metabolism in different environments. Among them, purine metabolic pathway was specific for the degradation of purine nucleosides by *L. brevis* PDD-5 in full targeted metabolic analysis (Figure 2A-D).

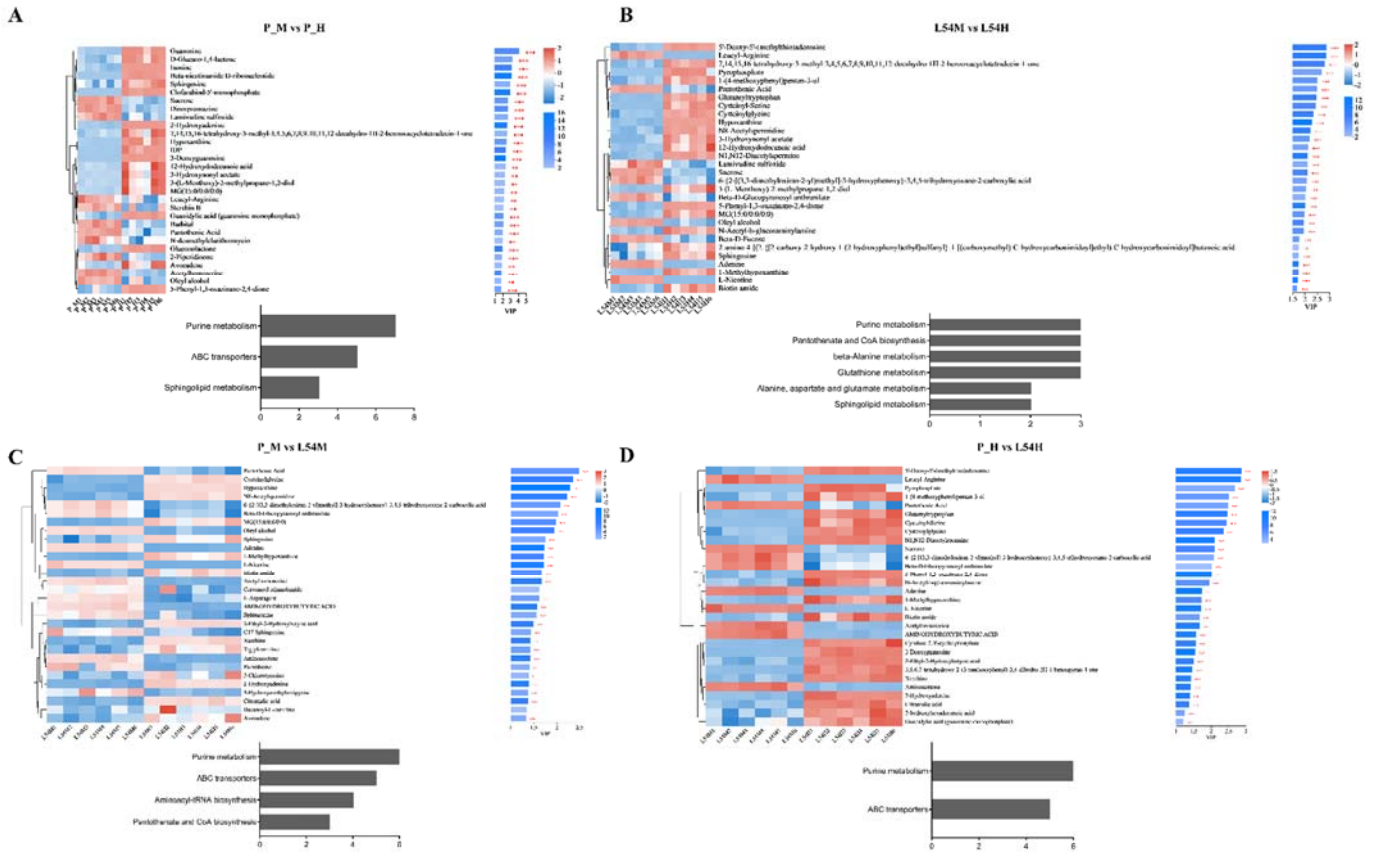

Figure 2. (A) Heat map of clustering between P_M and P_H, VIP value analysis and differential metabolite enrichment in the KEGG pathway. (B) Heat map of clustering between L54M and L54H, VIP value analysis and differential metabolite enrichment in the KEGG pathway. (C) Heat map of clustering between P_M and L54M, VIP value analysis and differential metabolite enrichment in the KEGG pathway. (D) Heat map of clustering between P_H and L54H, VIP value analysis and KEGG pathway for differential metabolite enrichment. P_M indicated untreated *L. brevis* PDD-5, P_H indicated *L. brevis* PDD-5 after inosine-guanosine buffer treatment, L54M indicated untreated *L. brevis* 54, and L54H indicated *L. brevis* 54 after inosine-guanosine buffer treatment.

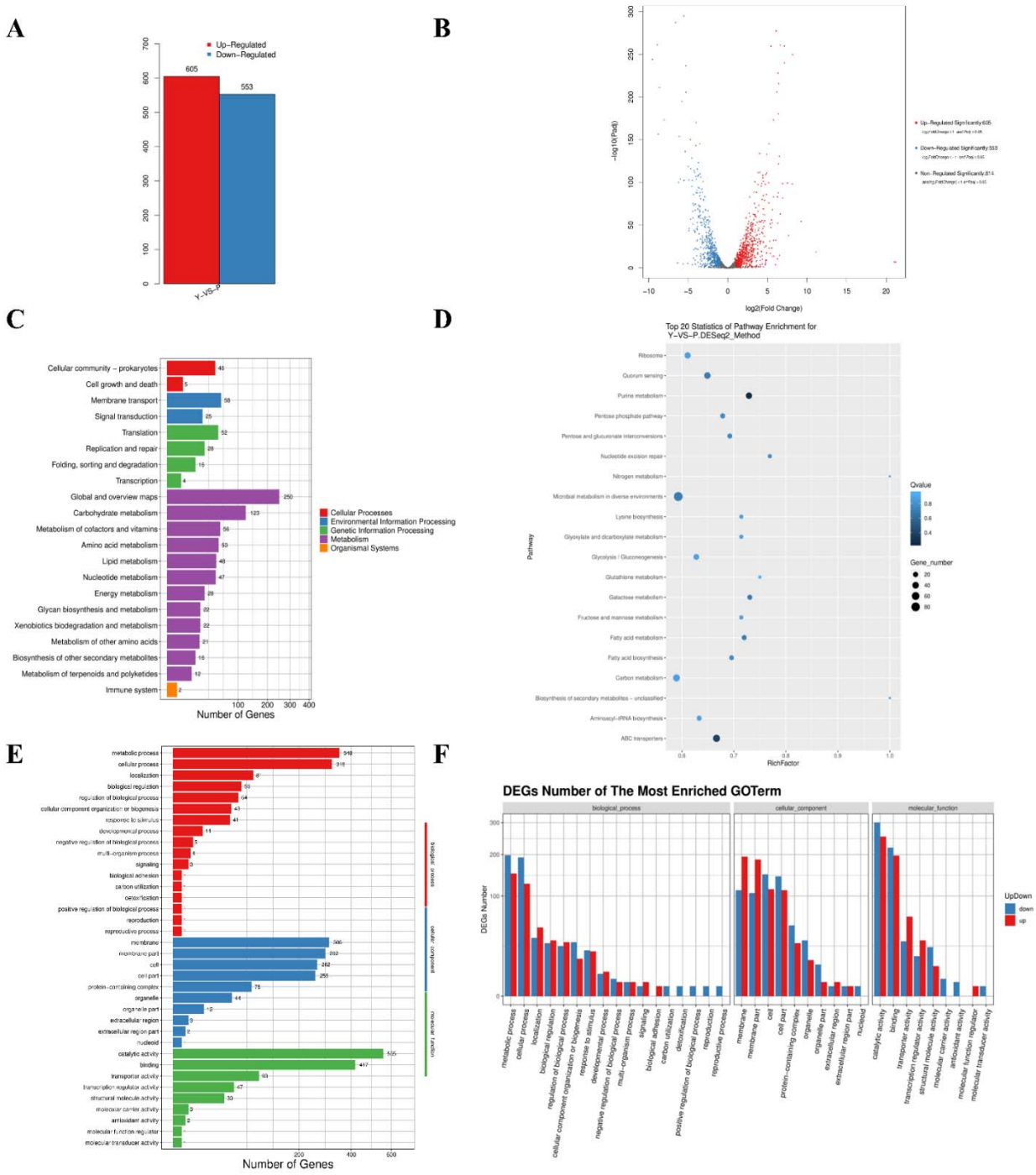

Figure 3. Analysis of *L. brevis* PDD-5 based on transcriptomics. (A) Statistical plot of significantly differentially expressed genes. Red represents up-regulation, blue represents down-regulation. (B) Volcano plot of differential genes. (C) Classification of KEGG pathway of significantly differentially expressed genes. (D) Pathway enrichment map of significantly differentially expressed genes. (E) GO functional classification of significantly differentially expressed genes. (F) GO functional classification of significantly up and down regulated differentially expressed genes.

Table 2. KEGG enrichment analysis of significantly differentially expressed genes in *L.brevis* PDD-5 and *L.brevis* ATCC 14869.

Pathway ID	Pathway	*P* value
ko00230	Purine metabolism	0.002
ko02010	ABC transporters	0.006
ko00052	Galactose metabolism	0.022
ko02024	Quorum sensing	0.029
ko01212	Fatty acid metabolism	0.031
ko01120	Microbial metabolism in diverse environment	0.035

Expression changes of key genes in *L. brevis* PDD-5, together with corresponding metabolite variations, were illustrated in Figure 4A based on KEGG annotation, and the associated genes and functional annotations are summarized in Table 3. Figure 4A illustrated that the pathway for purine nucleoside degradation into purines underwent significant alterations, with the gene *deoD*, encoding purine nucleoside phosphorylase [EC: 2.4.2.1], being upregulated in inosine and guanosine environments, leading to substantial conversion of nucleosides into purines. Additionally, in the *de novo* synthesis pathway, the expression of *deoB*, encoding phosphopentomutase [EC: 5.4.2.7], was enhanced, and the genes *PRPS* and *prsA*, encoding ribose-phosphate pyrophosphokinase [EC: 2.7.6.1], exhibited increased expression. The gene *purB*, encoding adenylosuccinate lyase [EC: 4.3.2.2], also showed elevated expression. During IMP degradation, the gene *gmpR*, encoding GMP reductase [EC: 1.7.1.7], and the gene *purA*, encoding adenylosuccinate synthase [EC: 6.3.4.4], both displayed significant increases in expression.

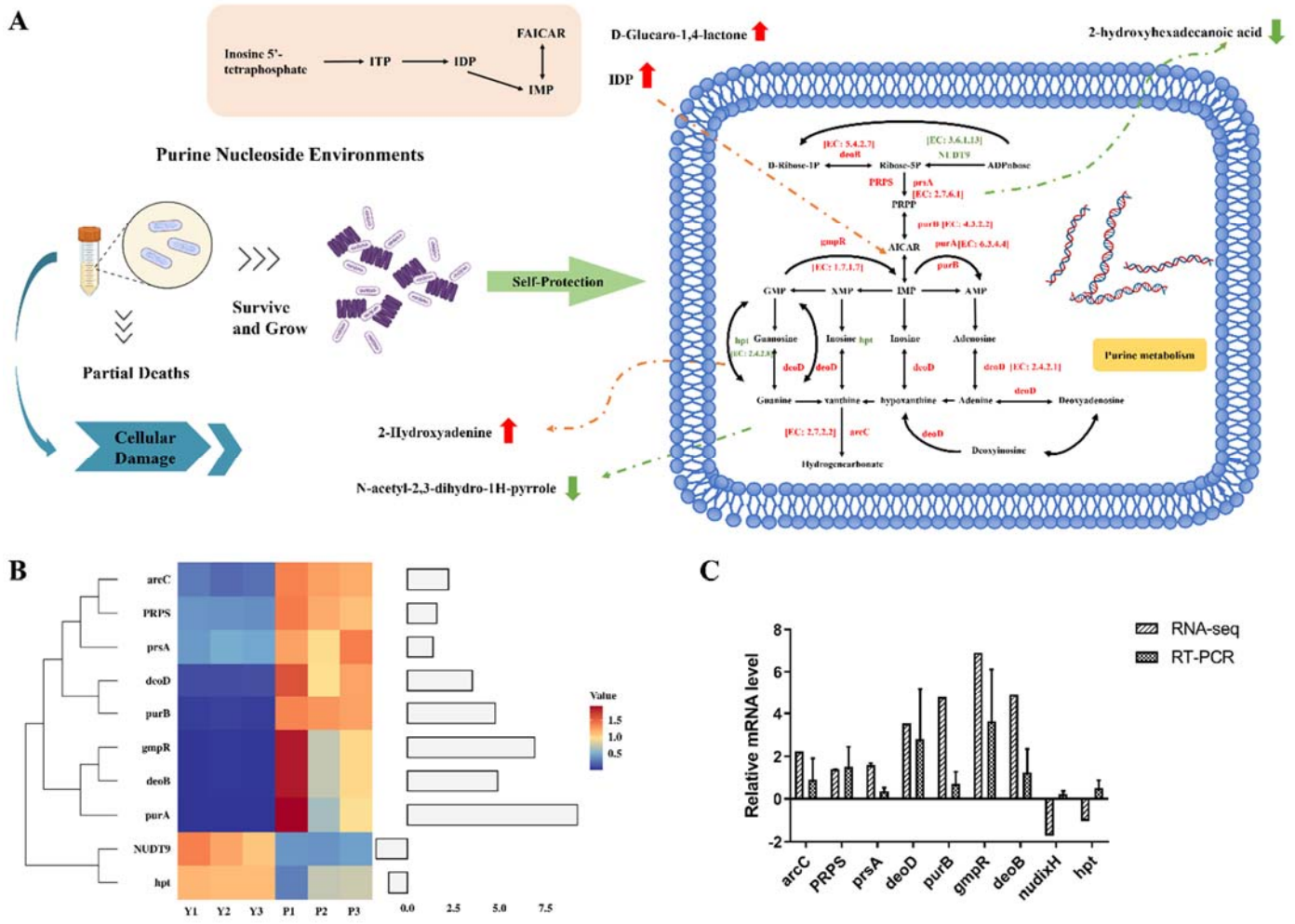

Figure 4. (A) Variations of key genes in the purine metabolism pathway in *L. brevis* PDD-5. Red letters indicated up-regulated genes and green letters indicated down-regulated genes. (B) Heat map analysis of key genes in the transcriptome. (C) Validation of key genes in *L. brevis* PDD-5. RNA-seq indicated the results of transcriptome sequencing of gene changes and qRT-PCR indicated the results of fluorescence quantification.

Table 3. Gene and function of *L. brevis* PDD-5 in purine metabolism pathway.

Gene ID	Definition	log2FoldChange(P/Y)
arcC	Carbamate kinase [EC:2.7.2.2]	2.23
deoD	Purine nucleoside pHospHorylase [EC:2.4.2.1]	3.53

deoB	Phosphopentomutase [EC:5.4.2.7]	4.90
gmpR	GMP reductase [EC:1.7.1.7]	6.91
hpt	Hypoxanthine phosphoribosyltransferase [EC:2.4.2.8]	-1.02
NUDT9	ADP-ribose pyrophosphatase [EC:3.6.1.13]	-1.71
purA	Adenylosuccinate synthase [EC:6.3.4.4]	9.25
purB	Adenylosuccinate lyase [EC:4.3.2.2]	4.78
PRPS	Ribose-phosphate pyrophosphokinase [EC:2.7.6.1]	1.59
prsA	Ribose-phosphate pyrophosphokinase [EC:2.7.6.1]	1.39

Furthermore, the transcriptional repressor *purR* (KO: K04751) showed a marked reduction in expression in the purine-treated group compared with the normal condition. The mean FPKM values of *purR* were 173.74 ± 6.09 in the Y group and 100.30 ± 14.00 in the P group (Welch's t = 8.33, df = 2.73, $P < 0.01$). Given that *purR* negatively regulates de novo purine biosynthetic genes, its downregulation likely relaxed transcriptional repression and contributed to the persistent activation of *de novo* purine synthesis despite extracellular purine abundance. This observation provided a regulatory explanation for the simultaneous enhancement of purine degradation and continued biosynthesis in *L. brevis* PDD-5. The differential expression of *purR* was shown in Table S6.

3.3 qRT-PCR analysis of the key genes in purine metabolism

To verify the differential gene results, gene expression changes of strain *L. brevis* PDD-5 were detected by qRT-PCR after purine nucleoside incubation, including genes *arcC*, *deoD*, *gmpR*, *hpt*, *NUDT9*, *deoB*, *purB*, *PRPS,* and *prsA*. The gene *gyrA* was designated as an internal reference gene. The primer designs were provided in Table 4. Figure S1 demonstrated the feasible design of the primers, which were not interfered with by dimerization. Figure 4B presented the results of gene expression in the validated transcriptome sequencing, and compared with the control, the gene expression trends were generally consistent with the sequencing results, except for the inconsistent expression of *hpt* and *NUDT9* genes.

Table 4. Primer sequences of genes in this study.

Gene ID	Primer sequence (5' to 3')
arcC	F: CTAAGGTCCAAGCCGCAATCAA
	R: TGTTCCATCGCCGTTCTTCAAG
deoD	F: CGTTCGGTGGTGGTATCTACTA
	R: GGGCTGTTGATTCCATTTCTGT
gmpR	F: GGAAGCCGTTCGTGAATTGGA
	R: GCAATGTCGCCGTTGTAGC
hpt	F: GGACCGAATCATCTGGGACGAT
	R: TTCCACGACCCGACCACTTG
NUDT9	F: GGTGACTCTGCTTCTCGTGAA
	R: CGGCTGGAATCTCTAATGTTGC
purA	F: AGAACTCACCTACCTCCACGAT
	R: CCGCTACCCGAATGCCAATT
phoS	F: GGCATGTGGCAGTTGGTTG
	R: GCTCGTCGGTTGTCTTGTG
purB	F: GGTCTGTGAGCAACTGGGAATC
	R: AGAACGCTGAAGGCTACGAATC
PRPS	F: GGCAATTCGGATTACGGTGTCA
	R: TCAATTCGTTGGGTCGCATCG
prsA	F: ATTGCTGACGAGGTTGGTGTTG
	R: CCGCCGTAACGCATCAATCATA

4. Discussion

Building on our previous work demonstrating that *L. brevis* PDD-5 effectively alleviates hyperuricemia by reducing serum uric acid levels and modulating renal urate transporters [7], this study aimed to elucidate the molecular mechanisms underlying its uric-acid-lowering capacity. To this end, the specificity of purine nucleoside degradation was compared between uric-acid-reducing and non-reducing *L. brevis* strains using full-targeted metabolomic analysis. The lack of separation between P_M and L54M indicated minimal metabolic differences under normal conditions, whereas the more pronounced metabolite variation between P_H and L54H reflected enhanced uptake and degradation of purine nucleosides by *L. brevis* PDD-5. These results were consistent with our previous physiological observations and support the notion that PDD-5 possesses a distinct metabolic advantage in purine-rich environments.

To further delineate these metabolic differences, a detailed comparative analysis of differential metabolites among all groups was conducted (Figure 1B). A total of 70 differential metabolites were identified between L54H and L54M, 75 metabolites between P_H and P_M, and 74 metabolites between P_H and L54H. In the purine metabolic pathway, the differential metabolites were inosine, guanosine, adenine, xanthine, IDP, and adenosine monophosphate in the P_H group compared to the L54H group. In addition, the sample correlation heat map (Figure 1C) reflected the similarity and abundance of metabolic composition between samples, with a clear separation between the metabolites of the strains in normal culture conditions (P_M and L54M) and those of the purine nucleoside treated strains (P_H and L54H), with no significant differences between the P_M and L54M groups, and differences between the purine nucleoside treated groups (P_H and L54H). This was consistent with the results of the PCA plot responses, and the data were reliable for each group of samples. Metabolite expression varied significantly among the four groups of samples, and the uric acid-lowering strains were clearly specific, thus focusing on the differential metabolites (Figure 1E). Xanthines, as one of the components of DNA and RNA, have important metabolic and signaling functions in cells [23], which represented that the nucleoside supplementation enhanced the growth of the strain. Xanthine was highly produced in the P_H and L54H groups and low in the P_M and L54M groups (Figure 1E). Moreover, Table S5 summarized the differential metabolites of P_H and L54H screened by VIP $\geq$ 1. On the one hand, the content of D-Glucaro-1,4-lactone was increased in the P_H group due to the fact that it is a metabolite of *L. brevis* PDD-5. On the other hand, D-Glucaro-1,4-lactone has been reported to be involved in detoxification metabolic pathways in the human body through the presence of similar detoxification metabolic mechanisms in microorganisms such as bacteria [24]. In a short period of time, the increase in D-Glucaro-1,4-lactone provided a carbon source for *L. brevis* PDD-5, and the threat of possible oxidative stress for the organism disappeared as the density of the bacterium grew. In particular, IDP is an intermediate metabolite in purine nucleotide metabolism that is elevated when *L. brevis* PDD-5 cells are subjected to DNA damage, such as oxidative stress. In addition, IDP is a metabolite in the transition state in some bacteria and yeast, so enhanced activity in specific metabolic pathways may lead to the accumulation of IDP, which provides a basis for subsequent studies of

metabolic pathways. Increased 2-Hydroxyadenine and 3-Deoxyguanosine were associated with the need for energy for strain growth and DNA damage [25].

In particular, 2-hydroxyhexadecanoic acid was an intermediate product of fatty acid metabolism [26], and when cells store energy, fatty acids combine into lipids to provide energy when needed. The significantly reduced metabolite 2-hydroxyhexadecanoic acid in the P_H group was probably related to cell growth. The reduction of N-acetyl-2,3-dihydro-1H-pyrrole was probably due to catabolism or oxidation of the prokaryotic acidification metabolic pathway into more stable metabolites [27], which is consistent with the possibility that *L. brevis* PDD-5 may have adapted to environmental uptake of degraded purine nucleosides through its own phage regulation.

Analysis of the degradation mechanism of purine nucleoside uptake by *L. brevis* PDD-5, only from metabolites, is not comprehensive. Combined omics analysis can provide a more comprehensive and deeper perspective for the exploration of the mechanisms of complex biological processes, so we continued to explore their specificity from a genetic perspective (Figure 3). Based on the results of GO and KEGG enrichment analyses of significantly different genes of *L. brevis* PDD-5 and *L. brevis* ATCC 14869 as described above, six significantly enriched pathways were screened for $P \leq 0.05$ threshold (Table 2). Among them, the purine metabolism pathway was specific for *L. brevis* PDD-5 degradation of purine nucleosides in full targeted metabolic analyses (Figure 2), which demonstrated the consistency and plausibility of the metabolome and transcriptome.

To probe deeply into the *in vitro* molecular mechanisms of uric acid-lowering LAB, we plotted Figure 4A. A combined analysis of key genes and critical metabolites was conducted (Figure 5). In the conversion of purine nucleosides to purines, purine nucleoside phosphorylase is one of the key enzymes in the purine remediation synthesis pathway [28]. There was typically a balance between the *de novo* synthesis of purine nucleosides and the remediation pathway, and the absence of the remediation pathway for purines would cause an increase in the rate of purine synthesis. Related research had clarified the absence of a remediation mechanism in some species of LAB [29], but not in *L. brevis*.

The gene *deoD* was upregulated, suggesting that *L. brevis* PDD-5 has an associated remediation pathway for purine nucleosides. In the purine nucleoside environment, upregulation of the gene *deoD* in *L. brevis* PDD-5 correlated with changes in metabolite IDP in full targeted metabolic outcomes, which were significantly increased in *L. brevis* PDD-5 compared to *L. brevis* 54 (Figure 2D), suggesting a strain-specific metabolic pathway for deoxyribonucleotides in *L. brevis*. In addition, a similar *deoD*-centered mechanism has been reported in the uric acid-lowering strain *Pediococcus acidilactici* GR-5. Ji *et al.* [30] demonstrated that *P. acidilactici* GR-5 alleviates hyperuricemia primarily through the upregulation of *deoD*, which catalyzes the phosphorolytic cleavage of purine nucleosides such as inosine, guanosine, and adenosine. This activity reduces intestinal absorption of purine nucleosides and subsequently lowers serum uric acid levels. GR-5 also modulated host inflammation by inhibiting the NLRP3 inflammasome, restoring tight-junction

proteins (Occludin and ZO-1), and elevating SCFA production, collectively contributing to systemic improvement in purine metabolism.

Our previous *in vivo* study confirmed that *L. brevis* PDD-5 exhibits similar physiological effects, including downregulation of URAT1 and GLUT9, upregulation of OAT1, and suppression of the NLRP3 pathway in hyperuricemic rats [7]. Therefore, *deoD*-mediated purine degradation and NLRP3 inhibition appear to represent a conserved mechanism among the most efficient uric acid-lowering LAB, such as *P. acidilactici* GR-5 and *L. brevis* PDD-5.

Notably, *L. brevis* PDD-5 and *L. brevis* 54 exhibited distinct physiological responses despite belonging to the same species. Preliminary metabolic profiling revealed that *L. brevis* 54 lacked uric-acid-lowering activity and showed no significant purine-nucleoside degradation *in vitro*, as determined by HPLC analysis. Consequently, transcriptomic analysis focused on *L. brevis* PDD-5 to elucidate the molecular basis underlying its unique urate-lowering phenotype. This design highlights strain-specific genetic regulation within *L. brevis*, emphasizing that uric-acid-lowering capacity is not a universal property but rather a strain-dependent adaptation.

Hypoxanthine phosphoribosyltransferase (HPRT) [EC: 2.4.2.8] is the enzyme that catalyzed the conversion of 5-phosphoribosyl-1-pyrophosphate to the corresponding mononucleotide and pyrophosphatase with hypoxanthine, guanine, and xanthine [31]. When inosine and guanosine were abundant, metabolism resulted in up-regulation of *deoD* gene expression and increased expression or activity of purine nucleoside phosphorylase [EC: 2.4.2.1]. The expression of *hpt*, the gene encoding HPRT [EC: 2.4.2.8], was repressed due to increased hypoxanthine and nucleoside metabolism and negative feedback [32] (Figure 4A). These findings were consistent with the results of the combined analysis presented in Figure 5.

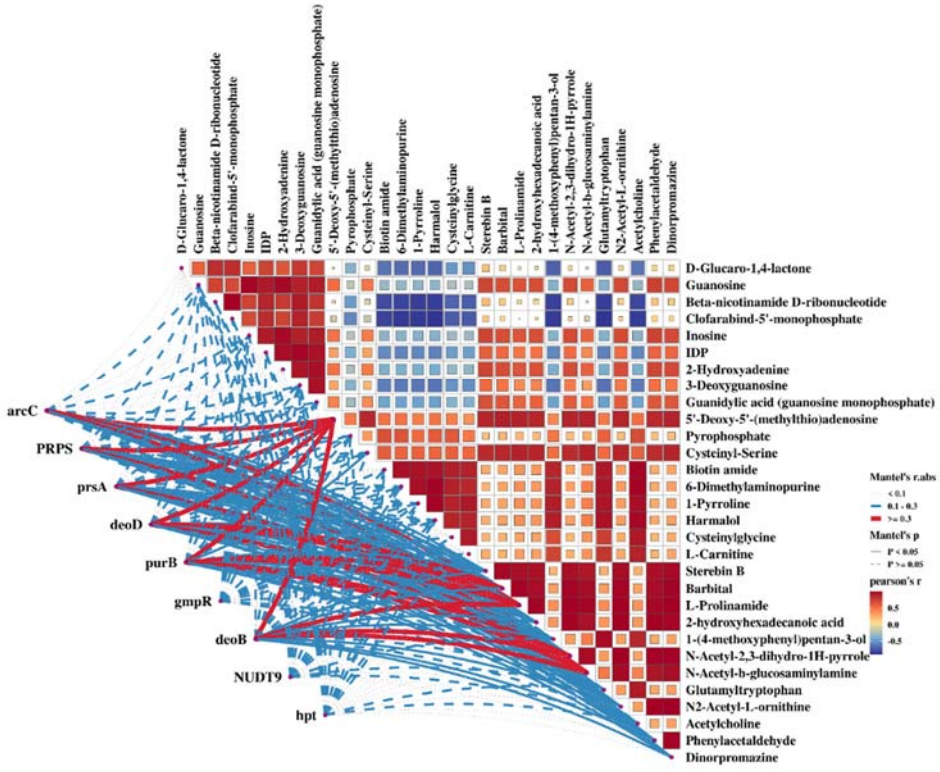

Figure 5. Correlation analysis of key genes and metabolites in uric acid-lowering lactic acid bacteria.

The *de novo* synthesis pathway of purines has been significantly altered. As a component of DNA and RNA, purine is one of the most abundant metabolites in the cell. The *de novo* synthesis of purines is a critical intracellular biosynthetic pathway that ensures adequate intracellular purine concentrations [33]. Phosphopentomutase [EC: 5.4.2.7], ribose-phosphate pyrophosphokinase [EC: 2.7.6.1], and adenylosuccinate lyase [EC: 4.3.2.2] are essential enzymes in the *de novo* synthesis pathway of purine nucleotides. phosphopentomutase [EC: 5.4.2.7], ribose-phosphate pyrophosphokinase [EC: 2.7.6.1], and adenylosuccinate lyase [EC: 4.3.2.2] are essential enzymes in the *de novo* synthesis pathway of purine nucleotides. The genes encoding these enzymes, *deoB*, *PRPS*, *prsA,* and *purB*, were upregulated, indicating an active purine *de novo* synthesis pathway in the purine nucleoside environment, which was associated with an increase in free hypoxanthine during purine degradation due to the upregulation of the gene *deoD*. Nonetheless, it was reported that the *de novo* synthesis pathway is usually silenced under conditions of excess purine or pyrimidine sources through a combination of protein inhibition and genetic regulation [29]. Interestingly, the transcriptional regulator *purR* (purine operon repressor, KO: K09685) was found to be significantly downregulated in the purine nucleoside environment compared with the normal condition. The mean expression levels of *purR* were 173.74 ± 6.09 in the Y group and 100.30 ± 14.00 in the P group ($P < 0.01$). As *PurR* acts as a negative regulator of the pur operon, its decreased expression would relieve transcriptional repression on *de novo* purine biosynthetic genes, thereby allowing continued activity of this pathway even under purine-rich conditions. This transcriptional pattern provided a mechanistic explanation for the observation that the *de novo* pathway remained active despite purine abundance in *L. brevis* PDD-5. These results indicated that downregulation of *purR* may represent a regulatory adaptation that enables *L. brevis* PDD-5 to maintain a balance between purine salvage and biosynthesis while efficiently metabolizing extracellular purine nucleosides.

Up-regulation of *deoB*, *PRPS*, and *prsA* gene expression may lead to an increase in certain pathways and related reactions in pentose phosphate metabolism and ribose metabolism. Therefore, changes in the expression of these genes may lead to the accumulation of metabolites such as D-Glucaro-1,4-lactone, 2-Hydroxyadenine, and 3-Deoxyguanosine (Figure 2D). In contrast, down-regulation of the gene *NUDT9* might be associated with an increase in inosine and guanosine, competitively inhibiting the activity of ADP-ribose pyrophosphatase [EC: 3.6.1.13]. Up-regulation of *purB* gene expression might suggest that certain pathways and related reactions in adenylate metabolism are increased, and therefore, in this case expression or activity of adenylosuccinate lyase [EC: 4.3.2.2] enzyme might be increased, resulting in a significant increase in adenylate metabolism, which could lead to other metabolites such as 2-hydroxyhexadecanoic acid and N-Acetyl-2,3-dihydro-1H pyrrole to accumulate or decrease.

Moreover, the up-regulation of the *arcC* gene could be aimed at increasing the synthesis of purine nucleotides of the purine metabolic pathway in *L. brevis* PDD-5 in an inosine and guanosine environment. *arcC* [EC: 2.7.2.2 carbamate kinase] is up-regulated by about 4.7-fold, which, on the one hand, probably means that *L. brevis* PDD-5 requires more AMP and GMP to meet the growth requirement. On the other

hand, the up-regulation of the gene *arcC* might have increased the rate of purine nucleotide biosynthesis to meet the purine nucleotide requirement of *L. brevis* PDD-5.

Interestingly, 2-hydroxyadenine is a DNA damage product generated under oxidative stress conditions [34]. In Figure 2D, the metabolism of 2-hydroxyadenine was increased in the *L. brevis* PDD-5 group and decreased in *L. brevis* 54, suggesting that *L. brevis* PDD-5 was more capable of surviving in a purine nucleoside-rich environment compared to *L. brevis* 54. The increase in 2-hydroxyadenine and the decrease in N-acetyl-2,3-dihydro-1H-pyrrole indicated that *L. brevis* PDD-5 possessed a strong ability to adapt to environmental challenges, as reflected by the increased IDP level (Figure 5). Furthermore, the elevated level of 2-hydroxyadenine suggested that *L. brevis* PDD-5 undergoes adaptive genomic or transcriptional responses to environmental stimuli, enabling the strain to efficiently utilize and metabolize purine nucleosides.

Purine *de novo* synthesis is an important route for the biosynthesis of purine nucleotides and involves the synergistic action of several enzymes [35]. IMP is an important intermediate in this process and plays an important role in the maintenance of life processes. IMP is synthesized by PRPP in 10 steps, and there are significantly different enzymes that catalyze this reaction in different microorganisms. Nygaard *et al.* [36] revealed that PurT enzyme was involved in the biosynthetic pathway of *E. coli*. However, the enzymes in the biosynthetic pathway of other bacteria were hardly studied, especially in Gram-positive bacteria [29]. Furthermore, *PurM*, *PurEK*, *PurC,* and *PurB* during *de novo* synthesis appear to be conserved in bacteria, but *PurR* enzymes are only required when PRPP is in sufficient supply [37]. As shown in Figure 4A, the *PurB* gene in *L. brevis* PDD-5 was essential only during *de novo* synthesis, which was a rather novel finding but still requires follow-up studies.

In the salvage pathway, it has been shown that *E. coli* can effectively use nucleosides as a source of carbon and energy by degrading the pentose portion of nucleosides [38]. A study on *Lactococcus lactis* (*L. lactis*) found that nucleosides were its only source of energy, and free nucleosides were transported into the cell and converted to ribulose-5-phosphate (*phoS*) through processes such as phosphorylation and recycled to PRPP (*PRPS* or *prsA*) and used for nucleotide formation [39], which was consistent with the results (Figure 4). In addition, the nucleotides are degraded into free bases, and the enzymes in this process are divided into purine nucleoside phosphorylase (*Pup*) and pyrimidine nucleoside phosphorylase (*Pdp*). Pup enzyme had been found to be present in *Bacillus subtilis* (*B. subtilis*), *E. coli,* and *L. lactis*, but due to controversial gene nomenclature in different strains [40], *Pup* in *B. subtilis* was changed to *deoCABD* in *E. coli* [41], corresponding to *deoD* in *L. lactis* IL1403. Figure 4B demonstrated that the *deoD* gene was present in *L. brevis* PDD-5 and played the same role. This was consistent with the results presented in Figure 5.

The opposite result we found for *hpt* in qRT-PCR might be due, on the one hand, to the fact that the hypoxanthine phosphoribosyltransferase encoded by the *hpt* gene also participates in the recycling pathway of purine nucleotides. On the other hand, the *hpt* is not only involved in the purine metabolism pathway but also in the purine nucleotide recycling pathway, so bioinformatics analysis on the huge RNA-Seq dataset

may produce some inaccurate results that cannot be matched with the qRT-PCR data. In addition, the *NUDT9* gene showed upregulation, although at a small fold, contrary to the transcriptome results, which may be related to the upregulation of the *deoB* gene, a key raw material in the purine *de novo* synthesis pathway, PRPP [42]. It was speculated from the transcriptome findings that free hypoxanthine increased the efficiency of PRPP synthesis, and the *NUDT9* synergized with the enzyme regulated by the *deoB* in order to produce PRPP. The transcriptome results showed a 4.9-fold up-regulation of *deoB* and an approximately 2-fold down-regulation of *NUDT9*. In contrast, the qRT-PCR results revealed that the *deoB* was up-regulated approximately two-fold less compared to the transcriptome results, and the *NUDT9* gene changed by the same fold. Hence, the gene changes of *L. brevis* PDD-5 were basically the same under the premise of receiving more inosine and guanosine. Overall, the results not only demonstrated the reliability and accuracy of transcriptome sequencing in gene expression studies, but also showed that these 9 genes played an important role in the degradation of purine nucleoside uptake by *L. brevis* PDD-5.

5. Conclusion

In summary, integrated targeted metabolomic and transcriptomic analyses were used to compare the purine nucleoside uptake and degradation capacities of *L. brevis* PDD-5 and *L. brevis* 54. Notably, *L. brevis* PDD-5 demonstrated a distinct preference for purine nucleoside utilization, as evidenced by enhanced activity in the purine metabolic pathway. Combined metabolic and transcriptional data suggest that *L. brevis* PDD-5 exhibited strong adaptability to purine-rich environments and may employ specific regulatory responses that enhance its capacity for purine uptake and degradation compared with *L. brevis* 54. These findings revealed the metabolic basis underlying the superior performance of *L. brevis* PDD-5 and provided a theoretical foundation for its potential application in microbial metabolic engineering and the development of novel biotechnological resources.

Conflict of Interest

We declare that we have no financial and personal relationships with other people or organizations that can inappropriately influence our work.

Availability of data and materials

Metabolomic data had been uploaded to the Metabolights website under the project name MTBLS7543. Transcriptome data for all six samples have been uploaded to the SRA database under submission number SUB13096375. biological project number PRJNA957069.

Acknowledgements

The authors thank the National Natural Science Foundation of China (32272339, 32402125, and 32360585).

References

[1] Zhang Y., et al., Fucoidan from Laminaria japonica Inhibits Expression of GLUT9 and URAT1 via PI3K/Akt, JNK and NF-κB Pathways in Uric Acid-Exposed HK-2 Cells. Mar Drugs. 19 (2021). https://doi.org/10.3390/md19050238.

[2] Tudela R., et al., Changes in RNA Catabolites of Sparkling Wines During the Biological Aging. Journal of Agricultural and Food Chemistry. 61 (2013) 6028-6035. https://doi.org/10.1021/jf4002582.

[3] Ragab G., Elshahaly M., Bardin T., Gout: An old disease in new perspective - A review. Journal of advanced research. 8 (2017) 495-511. https://doi.org/10.1016/j.jare.2017.04.008.

[4] Balasubramaniam S., Duley J.A., Christodoulou J., Inborn errors of purine metabolism: clinical update and therapies. Journal of Inherited Metabolic Disease. 37 (2014) 669-686. https://doi.org/10.1007/s10545-014-9731-6.

[5] Heeney D.D., Gareau M.G., Marco M.L., Intestinal Lactobacillus in health and disease, a driver or just along for the ride? Current Opinion in Biotechnology. 49 (2018) 140-147. https://doi.org/10.1016/j.copbio.2017.08.004.

[6] McLeod A., et al., Global transcriptome response in Lactobacillus sakei during growth on ribose. Bmc Microbiol. 11 (2011) 145. https://doi.org/10.1186/1471-2180-11-145.

[7] Xu J., et al., A novel strain of Levilactobacillus brevis PDD-5 isolated from salty vegetables has beneficial effects on hyperuricemia through anti-inflammation and improvement of kidney damage. Food Science and Human Wellness. 13 (2024) 898-908. https://doi.org/10.26599/FSHW.2022.9250077.

[8] Zhao H., et al., Ameliorative effect of *Lacticaseibacillus rhamnosus* Fmb14 from Chinese yogurt on hyperuricemia. Food Science and Human Wellness. 12 (2023) 1379-1390. https://doi.org/10.1016/j.fshw.2022.10.031.

[9] Yamada N., et al., PA-3 Uses the Purines IMP, Inosine and Hypoxanthine and Reduces Their Absorption in Rats. Microorganisms. 5 (2017). https://doi.org/1010.3390/microorganisms5010010.

[10] Wang H.N., et al., DM9218 ameliorates fructose-induced hyperuricemia through inosine degradation and manipulation of intestinal dysbiosis. Nutrition. 62 (2019) 63-73. https://doi.org/10.1016/j.nut.2018.11.018.

[11] Chen L., Zhong F., Zhu J., Bridging Targeted and Untargeted Mass Spectrometry-Based Metabolomics *via* Hybrid Approaches. Metabolites 10 (2020) 348. https://doi.org/10.3390/metabo10090348.

[12] Wang L. M., et al., 1H NMR and UHPLC/Q-Orbitrap-MS-Based Metabolomics Combined with 16S rRNA Gut Microbiota Analysis Revealed the Potential Regulation Mechanism of Nuciferine in Hyperuricemia Rats. J Agr Food Chem. 68 (2020) 14059-14070. https://doi.org/10.1021/acs.jafc.0c04985.

[13] Shi J., et al., Transcriptomic Responses to Nitrite Degradation by *Limosilactobacillus fermentum* RC4 and Effect of ndh Gene Overexpression on Nitrite Degradation. J Agr Food Chem. 71 (2023) 13156-13164. https://doi.org/10.1021/acs.jafc.3c03066.

[14] Caesar L.K., Kvalheim O.M., Cech N.B., Hierarchical cluster analysis of technical replicates to identify interferents in untargeted mass spectrometry metabolomics. Analytica Chimica Acta. 1021 (2018) 69-77. https://doi.org/10.1016/j.aca.2018.03.013.

[15] Buitrago D., et al., Impact of DNA methylation on 3D genome structure. Nat Commun. 12 (2021) 3243. https://doi.org/10.1038/s41467-021-23142-8.

[16] Yang L., et al., Transcriptomic and Metabolomic Profile Analysis of Muscles Reveals Pathways and Biomarkers Involved in Flavor Differences between Caged and Cage-Free Chickens. Foods. 11 (2022). https://doi.org/10.3390/foods11182890.

[17] Huang J., et al., Detection of Diseases Using Machine Learning Image Recognition Technology in Artificial Intelligence. Comput Intell Neurosci. 2022 (2022) 5658641. https://doi.org/10.1155/2022/5658641.

[18] Brouard C., et al., Fast metabolite identification with Input Output Kernel Regression. Bioinformatics. 32 (2016) i28-i36. https://doi.org/10.1093/bioinformatics/btw246.

[19] Liu J., et al., miR-125b promotes MLL-AF9-driven murine acute myeloid leukemia involving a VEGFA-mediated non-cell-intrinsic mechanism. Blood. 129 (2017) 1491-1502. https://doi.org/10.1182/blood-2016-06-721027.

[20] Lamarre S., et al., Optimization of an RNA-Seq Differential Gene Expression Analysis Depending on Biological Replicate Number and Library Size. Frontiers in Plant Science. 9 (2018) 108. https://doi.org/10.3389/fpls.2018.00108.

[21] Lin H., et al., Investigation into the potential mechanism of Bacillus amyloliquefaciens in the fermentation of broad bean paste by metabolomics and transcriptomics. Food Research International. 183 (2024) 114202. https://doi.org/10.1016/j.foodres.2024.114202.

[22] Sun Z., et al., High-concentration Mg^{2+} stress improves L-lactic acid biosynthesis of Bacillus coagulans revealed by combined analysis of transcriptome and metabolome. Journal of Biotechnology. 409 (2026) 1-13. https://doi.org/https://doi.org/10.1016/j.jbiotec.2025.09.016.

[23] Perchellet J.-P., Boutwell R.K., Comparison of the effects of 3-isobutyl-1-methylxanthine and adenosine cyclic 3':5' -monophosphate on the induction of skin tumors by the initiation-promotion protocol and by the complete carcinogenesis process. Carcinogenesis. 3 (1982) 53-60. https://doi.org/10.1093/carcin/3.1.53.

[24] Walaszek Z., Potential use of d-glucaric acid derivatives in cancer prevention. Cancer Letters. 54 (1990) 1-8. https://doi.org/10.1016/0304-3835(90)90083-A.

[25] Tsurudome Y., et al., 2-Hydroxyadenine, a mutagenic form of oxidative DNA damage, is not repaired by a glycosylase type mechanism in rat organs. Mutation Research/DNA Repair. 408 (1998) 121-127. https://doi.org/https://doi.org/10.1016/S0921-8777(98)00025-1.

[26] Lanz C., et al., The production and composition of rat sebum is unaffected by 3 Gy gamma radiation. International journal of radiation biology. 87 (2011) 360-371. https://doi.org/10.3109/09553002.2010.537432.

[27] Price M.N., et al., Oxidative Pathways of Deoxyribose and Deoxyribonate Catabolism. 4 (2019) 10.1128/msystems.00297-00218. https://doi.org/doi:10.1128/msystems.00297-18.

[28] Lerman J.A., et al., In silico method for modelling metabolism and gene product expression at genome scale. Nature Communications. 3 (2012) 929. https://doi.org/10.1038/ncomms1928.

[29] Kilstrup M., et al., Nucleotide metabolism and its control in lactic acid bacteria. FEMS Microbiology Reviews. 29 (2005) 555-590. https://doi.org/10.1016/j.fmrre.2005.04.006.

[30] Ji J., et al., Pediococcus acidilactici GR-5 alleviates hyperuricemia by degrading purine nucleosides and improving gut microbiota metabolism. npj Science of Food. 9 (2025) 183. https://doi.org/10.1038/s41538-025-00556-y.

[31] Wu J., et al., HIF-1α in the heart: remodeling nucleotide metabolism. Journal of molecular and cellular cardiology. 82 (2015) 194-200. https://doi.org/10.1016/j.yjmcc.2015.01.014.

[32] Sauro H.M., Control and regulation of pathways via negative feedback. 14 (2017) 20160848. https://doi.org/doi:10.1098/rsif.2016.0848.

[33] Pareek V., et al., Metabolomics and mass spectrometry imaging reveal channeled de novo purine synthesis in cells. Science. 368 (2020) 283-290. https://doi.org/10.1126/science.aaz6465.

[34] Valavanidis A., Vlachogianni T., Fiotakis C., 8-hydroxy-2′ -deoxyguanosine (8-OHdG): A Critical Biomarker of Oxidative Stress and Carcinogenesis. Journal of Environmental Science and Health, Part C. 27 (2009) 120-139. https://doi.org/10.1080/10590500902885684.

[35] Jurecka A., Inborn errors of purine and pyrimidine metabolism. Molecular Genetics and Metabolism. 32 (2009) 164-176. https://doi.org/10.1007/s10545-009-1094-z.

[36] Nygaard P., Smith J.M., Evidence for a novel glycinamide ribonucleotide transformylase in Escherichia coli. J Bacteriol. 175 (1993) 3591-3597. https://doi.org/10.1128/jb.175.11.3591-3597.1993.

[37] Kilstrup M., Martinussen J., A Transcriptional Activator, Homologous to the Bacillus subtilis PurR Repressor, Is Required for Expression of Purine Biosynthetic Genes inLactococcus lactis. J Bacteriol. 180 (1998) 3907-3916. https://doi.org/10.1128/JB.180.15.3907-3916.1998.

[38] Rocchietti S., et al., Immobilization and stabilization of recombinant multimeric uridine and purine nucleoside phosphorylases from Bacillus subtilis. Biomacromolecules. 5 (2004) 2195-2200. https://doi.org/10.1021/bm049765f.

[39] Bolotin A., et al., The complete genome sequence of the lactic acid bacterium Lactococcus lactis ssp lactis IL1403. Genome Research. 11 (2001) 731-753. https://doi.org/10.1101/gr.GR-1697R.

[40] Mohlmann T., et al., Nucleoside transport and associated metabolism. Plant Biology. 12 (2010) 26-34. https://doi.org/10.1111/j.1438-8677.2010.00351.x.

[41] Hammer-Jespersen K., et al., Induction of Enzymes Involved in the Catabolism of Deoxyribonucleosides and Ribonucleosides in *Escherichia coli* K 12. European journal of biochemistry. 19 (1971) 533-538. https://doi.org/10.1111/j.1432-1033.1971.tb01345.x.

[42] Kim P.B., Nelson J.W., Breaker R.R., An ancient riboswitch class in bacteria regulates purine biosynthesis and one-carbon metabolism. Molecular cell. 57 (2015) 317-328. https://doi.org/10.1016/j.molcel.2015.01.001.